remote sensing

Article

Land Subsidence Detection Using SBAS- and Stacking-InSAR with Zonal Statistics and Topographic Correlations in Lakhra Coal Mines, Pakistan

Tariq Ashraf [1], Fang Yin [2,*], Lei Liu [1] and Qunjia Zhang [1]

[1] School of Earth Science and Resources, Chang'an University, Xi'an 710054, China; tariqashrafcumt@gmail.com (T.A.); liul@chd.edu.cn (L.L.); qunjiazhang@chd.edu.cn (Q.Z.)
[2] School of Land Engineering, Chang'an University, Xi'an 710054, China
* Correspondence: yinf@chd.edu.cn

Abstract: The adverse combination of excessive mining practices and the resulting land subsidence is a significant obstacle to the sustainable growth and stability of regions associated with mining activities. The Lakhra coal mines, which contain some of Pakistan's largest coal deposits, have been overlooked in land subsidence monitoring, indicating a considerable oversight in the region. Subsidence in mining areas can be spotted early when using Interferometric Synthetic Aperture Radar (InSAR), which can precisely monitor ground changes over time. This study is the first to employ the Small Baseline Subset (SBAS)-InSAR and stacking-InSAR techniques to identify land subsidence at the Lakhra coal mines. This research offers critical insights into subsidence mechanisms in the study area, which has never been previously investigated for ground deformation monitoring, by utilizing 150 Sentinel-1A (ascending) images obtained between January 2018 and September 2023. A total of 102 deformation spots were identified using SBAS-InSAR, while stacking-InSAR detected 73 deformation locations. The most extensive cumulative subsidence in the Lakhra coal mine was −114 mm, according to SBAS-InSAR, with a standard deviation of 6.63 mm. In comparison, a subsidence rate of −19 mm/year was reported using stacking-InSAR with a standard deviation of 1.17 mm/year. The rangeland covered 88.8% of the total area and exhibited the most significant deformation values, as determined by stacking and SBAS-InSAR techniques. Linear regression showed that there was not a strong correlation between subsidence and topographic factors. As detected by optical remote sensing data, the subsidence locations were near or above the mines in the research area, indicating that widespread mining in Lakhra coal mines was the cause of subsidence. Our findings suggest that SAR interferometric time series analysis is helpful for proactively identifying and controlling subsidence difficulties in mining regions by closely monitoring activities, hence reducing negative consequences on operations and the environment.

Keywords: SBAS-InSAR; stacking-InSAR; Lakhra coal mines; mining subsidence; zonal statistics

check for updates

Citation: Ashraf, T.; Yin, F.; Liu, L.; Zhang, Q. Land Subsidence Detection Using SBAS- and Stacking-InSAR with Zonal Statistics and Topographic Correlations in Lakhra Coal Mines, Pakistan. *Remote Sens.* **2024**, *16*, 3815. https://doi.org/10.3390/rs16203815

Academic Editor: Deodato Tapete

Received: 27 August 2024
Revised: 5 October 2024
Accepted: 11 October 2024
Published: 14 October 2024

1. Introduction

Land subsidence monitoring is critical for managing and mitigating the risks associated with infrastructure damage, ecosystem disruption, and human safety. In some cases, subsidence can result in permanent land loss, which can have significant economic and social implications for communities that rely on the land for agriculture, housing, and livelihood purposes. Monitoring land subsidence is crucial for understanding its causes, assessing risks, and implementing mitigation measures [1,2].

Traditional methods for monitoring land subsidence, such as ground leveling and GPS techniques, are often single-point measurements, which are inefficient and unsuitable for large-scale implementation. These techniques also require significant investments in workforce and material resources while setting and implementing monitoring point density, network range, and measurement frequency [3,4]. Interferometric Synthetic Aperture

Radar (InSAR) has been instrumental in this regard, providing valuable insights into the spatiotemporal variations in surface deformation [5]. InSAR can offer extensive spatial coverage, exceptional imaging resolution, and non-invasive surveying [6]. Preliminary research has shown that InSAR can identify and chart occurrences of land subsidence. E.J. Fielding et al. [7] recorded maximum subsidence rates of 35 days of approximately 40 mm and 400 mm annually in the Lost Hills and Belridge oilfields of California's San Joaquin Valley. Gabriel et al. [8] devised differential radar interferometry (D-InSAR), effectively differentiating between ground elevation and deformation signals.

Nevertheless, the D-InSAR approach frequently encounters interference from atmospheric factors and spatiotemporal decorrelation distortion [9,10]. According to Ferretti et al. [11,12], a pixel's phase stability is improved when its amplitude deviation falls within a specific range. These specific pixels are referred to as persistent scatterers (PSs). Contrary to Persistent Scatterer Interferometry (PSI), ref. [13] created a sequence of interferograms with small spatiotemporal baselines. The SBAS (Small Baseline Subset) approach exhibits distinct characteristics compared to D-InSAR. The SBAS-InSAR technique performs time-series analysis by employing a sequence of radar images acquired over time to assess and analyze ground deformation. This approach emphasizes the selection of image pairs with minimal temporal and spatial baselines to improve the sensitivity when identifying gradual surface displacements. Compared to the Persistent Scatterer InSAR (PS-InSAR) technique, SBAS-InSAR has the advantages of overcoming the decorrelation of high distortion rate regions and decreasing the noise in displacement time-series analyses [14,15]. Furthermore, it exclusively captures signals emanating from locations that exhibit consistent scattering patterns [16]. This technique enhances the precision of deformation extraction. Small Baseline Subset InSAR is a valuable tool for various geodetic fields, such as ground subsidence [17–19], landslides [19–21], and seismic activity [22,23]. SBAS-InSAR is an effective approach employed to monitor the integrity of infrastructure and land subsidence in urban areas, with a particular emphasis on vulnerable areas. This technique improves natural hazard assessments by facilitating the identification of ground deformation prior to earthquakes and landslides. It evaluates the integrity of critical infrastructure for timely maintenance while ensuring safety in mining regions through ground displacement monitoring. Furthermore, SBAS-InSAR monitors environmental changes associated with climate impacts and land utilization, thereby facilitating the development of effective policies and management.

Research has shown that SBAS-InSAR technology can obtain reliable and accurate results in regions with different deformation characteristics, and its application has significantly improved the monitoring accuracy of mining surface deformation [5,24,25].

The stacking-InSAR technique is a simple yet efficient method to measure the mean mining subsidence velocity in the line-of-sight (LOS) direction. This technique takes several unwrapped interferograms and weights them according to the period, which helps to fulfill the requirements of long-term mining subsidence monitoring while reducing the impacts of atmospheric phase screens [26–29]. Qin et al. employed stacking-InSAR and a 3D model using the finite difference approach to observe ground deformation in the Fang Zhuang coalfield in 2016. The scholars determined that mining activities were the primary source of the deformation and that the spatial distribution was influenced by geological faults in the area of investigation [30]. In the Wuda coalfield (northern China), Jiang et al. used stacking, persistent scatterer interferometry, and two-pass D-InSAR methods to uncover the spatiotemporal details of land subsidence in regions ravaged by coal fires. Their findings agreed with GPS observations and data collected from coal fires in the region [31]. Zhu et al. utilized the stacking-InSAR technique to identify active landslides in the western region of Guizhou, characterized by serried vegetation and precipitous topography. These landslides encompass natural occurrences, reservoir-induced events, and those triggered by mining activities [32].

Mining operations have the potential to cause subsidence, a phenomenon that might manifest days or even decades after the commencement of extraction [33,34]. The extensive mining operations in the Lakhra coal mines in Sindh, Pakistan, which consist of more than 400 mines, constitute a substantial portion of Pakistan's coal reserves. Considering the magnitude of these activities, the extraction technologies used have the potential to cause land subsidence. Failing to notice subsidence may result in infrastructure malfunctions, destruction of the environment, tardy response, legal liability, poor land use planning, and a loss of public trust. This challenge highlights the crucial need to establish robust monitoring systems to evaluate and reduce the risks associated with subsidence in this area. The lack of monitoring procedures in this field highlights a notable research gap, which calls for a concentrated investigation into the dynamics of subsidence events.

This study uses the sophisticated SBAS-InSAR and stacking-InSAR technique to analyze 150 Sentinel-1A images taken between January 2018 and September 2023. The investigation is centered on the Lakhra coal mines area in the Sindh province of Pakistan to identify any occurrences of mining subsidence in the region. The zonal statistics of the area are calculated, the land subsidence characteristics under various land cover types are observed, and the correlation between topographic features and deformation is also established. Optical remote sensing images taken from Google Earth Pro version 7.3 evaluate the potential factors contributing to land subsidence. The findings can be a conceptual foundation for establishing regional rules and safety protocols for mining operations in the area.

2. Materials and Methods

2.1. Study Area

The Lakhra coal field, situated in Sindh Province approximately 32 km northwest of the historic city of Hyderabad, lies on the western bank of the Indus River Valley within the southern region of Pakistan. Our area of interest geographically lies in the latitude range of approximately 25.43 to 25.95 and the longitude range of approximately 67.85 to 68.37 degrees (Figure 1). The topography of the area of interest ranges from 26 to 207 m, with most of the region spanning between 98 and 138 m.

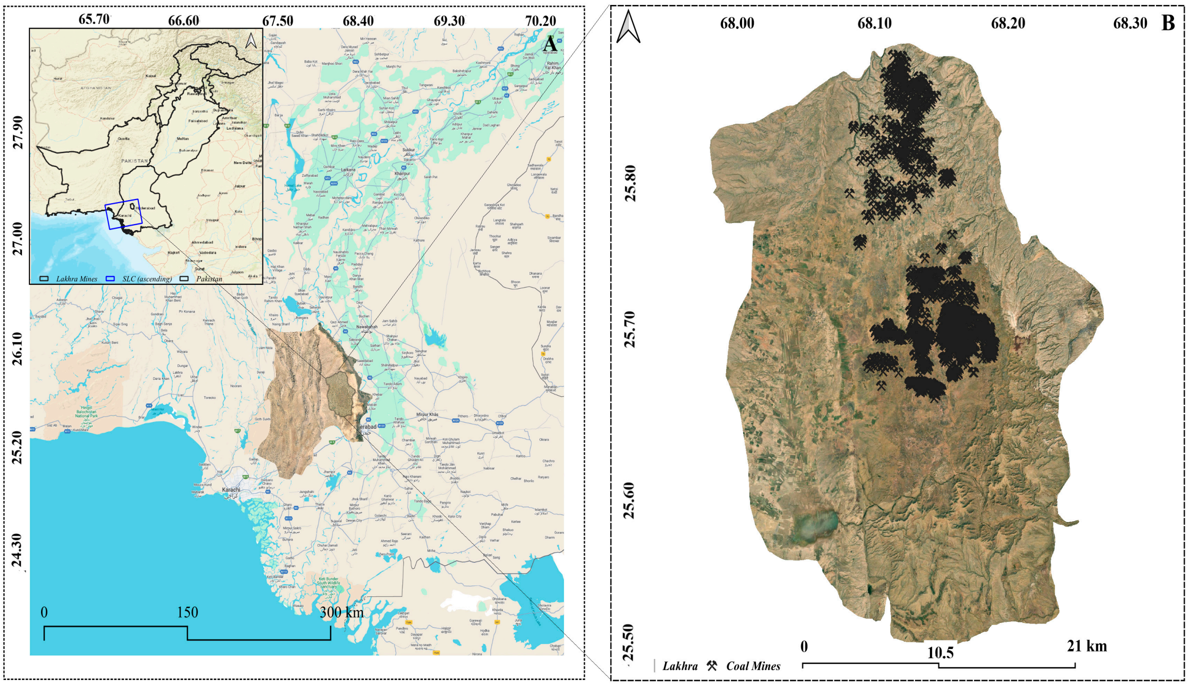

Figure 1. Location of the Study Area Lakhra Mines. (**A**) Top left corner shapefile of Pakistan and area showing Sindh province where Lakhra mines are located. (**B**) Area of Interest zoomed view.

Coal deposits are located within the mild Lakhra anticline. The coal is located between 50 from 150 m [35]. The mining industry consistently engenders environmental consequences, including the depletion of biodiversity, the creation of sinkholes, ecological degradation, and the pollution of water, groundwater, and soil [36]. Several locations to the east and south exhibit the most elevated topography, ranging from 170 to 207 m (Figure 2A). The region is predominantly characterized by rangeland and bare landscapes, with limited built-up areas and patches of farmed land. Notably, water bodies are sparse, occupying only a tiny percentage of the land (Figure 2B). The Lakhra coal mines area contains more than 400 coal mines, as observed through Google Earth; the underground chamber and pillar mining technology are used to mine the coal. In the Paleocene Bara Formation, lignite coal reserves amount to a total of 1.328 billion tons.

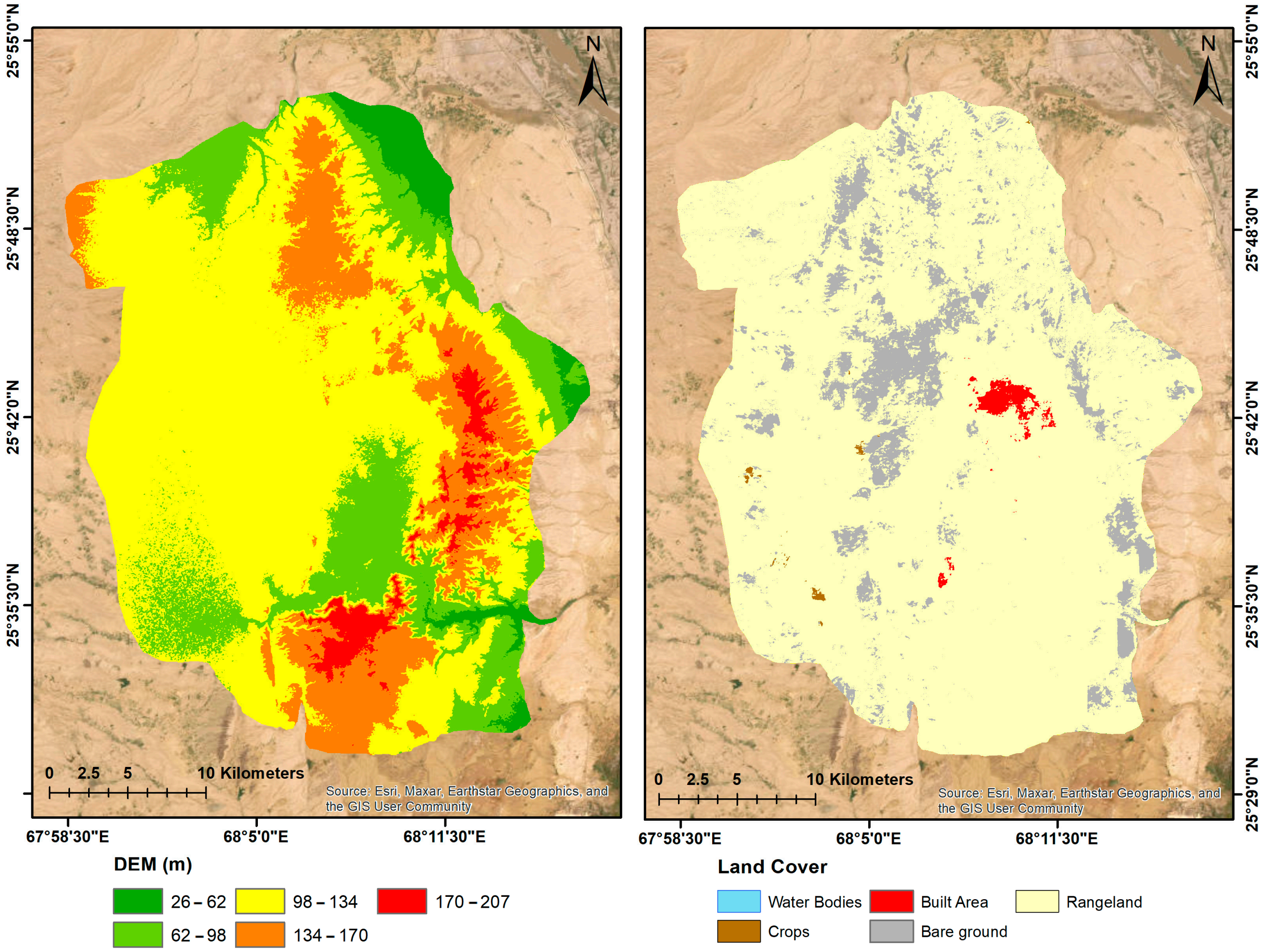

(**A**) (**B**)

Figure 2. (**A**) Digital Elevation Model of the Study Area. (**B**) Land Cover Map.

2.2. Dataset

The dataset for this study comprises 150 Sentinel-1 Synthetic Aperture Radar Single Look Complex (SLC) ascending track images acquired between 8 January 2018 and 15 September 2023 to monitor the land deformation in the Lakhra coal field. The dataset comprises the SLC Level 1 product obtained in Interferometric Wide Swath (IW) mode. This dataset encompasses 250 km of surface data with a 5 × 20 m spatial resolution. Furthermore, it includes amplitude and phase information, enabling detailed analysis of terrain features and monitoring various environmental phenomena [37]. These images were sourced on 10 November 2023 from the Alaska Satellite Facility (ASF) Distributed Active Archive Center (DAAC) (https://search.asf.alaska.edu accessed on 10 November 2023), known for its comprehensive SAR data collection. The Sentinel-1 SLC C band images utilized in this research offer high-resolution radar data captured at a wavelength of approximately 5.6 cm. C-band imaging radars are typically unaffected by atmospheric conditions and can see through tropical clouds and rain showers [38]. The radar's capability to penetrate vegetation canopies or soils is limited to the top layers. The Shuttle Radar Topography Mission (SRTM) 1 Arc-Second Global DEM data with a spatial resolution of 30 m, obtained from the USGS Earth Explorer website (https://earthexplore.usgs.gov/ accessed on 10 November 2023), were utilized to generate slopes and aspect maps of the study area and to remove topographic and flattening phases during InSAR processing. The land cover categorization is based on the authoritative Esri 2020 Global Land Cover dataset (https://www.arcgis.com/apps/instant/media/index.html?appid=fc92d38533d440078f17678ebc20e8e2 accessed on 10 November 2023), which provides a solid platform for assessing environmental composition and spatial changes. Esri's 2020 layer of land cover is a comprehensive worldwide map of land use and land cover (LULC) obtained from ESA Sentinel-2 images with a resolution of 10 m. It is a deep learning model's composite of land use and land cover predictions for ten classes. It is trained on over five billion manually labeled Sentinel-2 pixels from over 20,000 sites spread throughout the world's major biomes.

2.3. InSAR Process

The SBAS approach enhances the spatial extent for extracting dependable phase delay time series, particularly in non-urban regions, by considering the speckle characteristics of most targets in the Synthetic Aperture Radar images [39–41]. The fundamental ideas, operational protocols, and attributes of SBAS-InSAR have been thoroughly documented in previous research [42–44] and will not be reiterated in detail here. However, a general workflow is presented in Figure 3. The processing was carried out using GAMMA-2017® software developed by GAMMA remote sensing AG, Muri bei Bern, Switzerland [45]. The preprocessing steps involved transcribing and modifying data and SLC parameter file generation, calibration, multi-looking, cropping of SLC, and co-registration. The image 20,201,105 was selected as the master image by the freely available Sentinel Application Platform SNAP (https://step.esa.int/snap/ accessed on 10 November 2023) version 9.0.0. The Earth's surface can undergo natural and human-caused alterations over extended time intervals or broad spatial baselines, resulting in decorrelation between the reference and slave images. To mitigate the effects of these shifts and enhance the quality of the interferogram, we employed small spatial and temporal baselines of 150 m and 60 days, respectively, generating 571 interferograms of the area of interest. Figure 4 shows the average spatial coherence and network of interferograms generated using the above-mentioned spatiotemporal baseline. It is evident from Figure 4 that all of the interferograms show good average spatial coherence. Interferograms are a redundant network connecting images in the spatiotemporal baseline space.

After selecting interferogram pairs, SRTM DEM eliminated the topographic and flattening phases and InSAR product geocoding. Subsequently, adaptive filtering and phase unwrapping were employed to acquire a sequence of unwrapped differential interferograms. Ultimately, for each random pixel (x, y) in interferogram I (produced by SAR images captured at times t1 and t2), the value can be represented as Equation (1):

$$\varphi diff = \varphi def + \varphi topo_{res} + \varphi atm_{res} + \varphi noise \tag{1}$$

where $\varphi def + \varphi topo_{res} + \varphi atm_{res} + \varphi noise$ reflects the phase of ground deformation, terrain errors, residual atmospheric artifacts, and decorrelation/thermal noise. The unwrapped differential interferometric phases, which are primarily deformation phases after the other phase component has been eliminated or attenuated, can be multiplied by a constant factor to turn them into surface displacement.

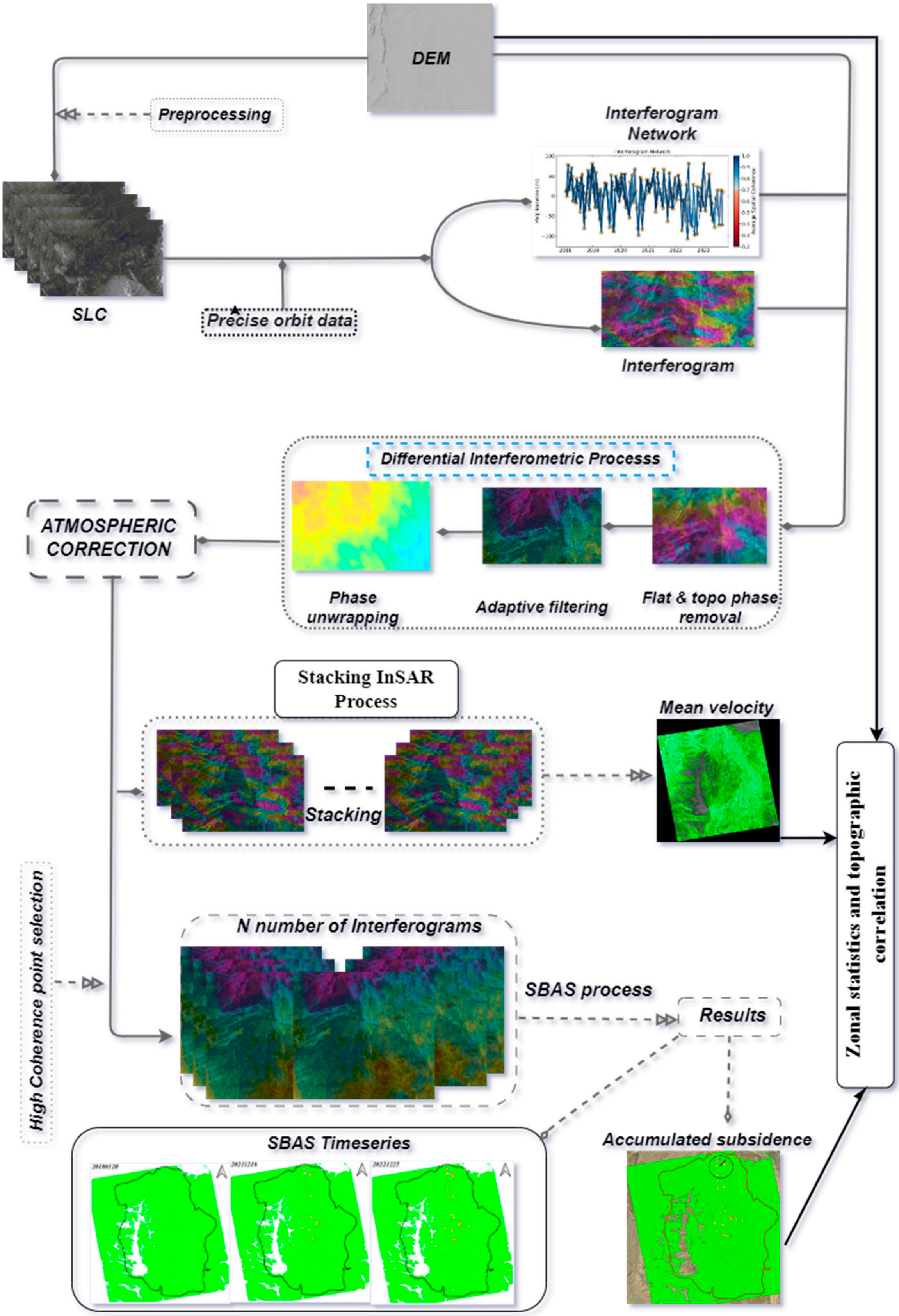

Figure 3. SBAS- and Stacking-InSAR Workflow.

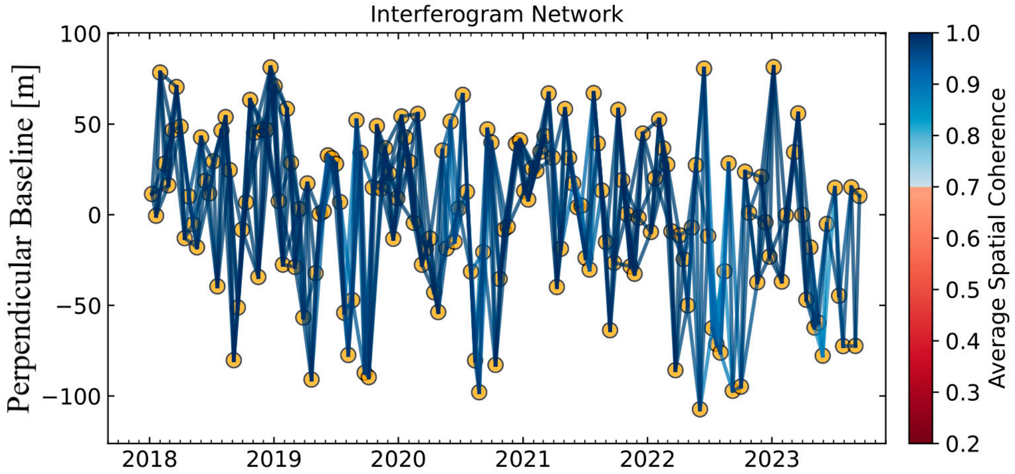

Figure 4. Interferogram Network and Average Spatial Coherence.

Stacking-InSAR, or interferogram stacking, is a time-series method employed in InSAR. It is a sophisticated technique that calculates linear displacement using a collection of unwrapped differential interferograms. The unwrapped phases of a sequence of interferograms are combined and weighted to enhance the signal-to-noise ratio (SNR) in the stacking phase and minimize the impact of noise.

The calculation of the mean displacement rate along with its standard deviation is achievable by considering the significance of the time span for each interferogram as Equation (2):

$$v_{mean} = \frac{\lambda}{4\pi} \cdot \frac{\sum_{\beth=1}^{N} \varphi_i \Delta T_i}{\sum_{i=1}^{N} \Delta T_i^2} \tag{2}$$

The formula calculates the yearly average deformation rate along the line-of-sight (LOS) direction, denoted as v_{mean}. This calculation uses the interferogram's unwrapped phase φ_i. The timeline baseline ΔT is associated with the interferogram and the total number of interferograms stacked N. The singular value decomposition approach calculated the deformation results within the SBAS-InSAR time series. When using SBAS-InSAR to model deformation velocity, it is crucial to account for topographic and atmospheric phase errors. This process ensures the reliability of the obtained results. SBAS-InSAR often overlooks points exhibiting low temporal coherence, which leads to a reduced point density compared to the stacking-InSAR method.

3. Results

3.1. Stacking-InSAR Results

Figure 5 displays the monitoring outcome obtained by the stacking-InSAR technique. The stacking procedure involved 500 interferograms. The red hue signifies subsidence, which is the movement in the direction of the satellite's line of sight. The blue color signifies uplift, which is the movement toward the satellite's LOS. The rest of the colors show the values as the color ramp represents in Figure 5A. The blank patches indicate missing data owing to decoherence.

The red polygon in Figure 5A shows the area of interest. Figure 5B provides a magnified view of the deformation, whereas Figure 5C displays the profile plot of the subsidence along the line (AB), showing a subsidence rate reaching −16 mm/year. While subsidence is evident in the area, a few spots are uplifted. The maximum subsidence rate recorded through stacking-InSAR analysis is −19 mm/year, while the highest uplift rate observed reaches 6.8 mm/year. To better understand the results, the area showing obvious deformation is divided into two sections: the upper area of Lakhra mines toward the North, referred to as Upper Lakhra (UL), defined by a black rectangle, and the location of Lakhra mines marked by a blue rectangle, referred to as Lower Lakhra (LL) (Figure 5A).

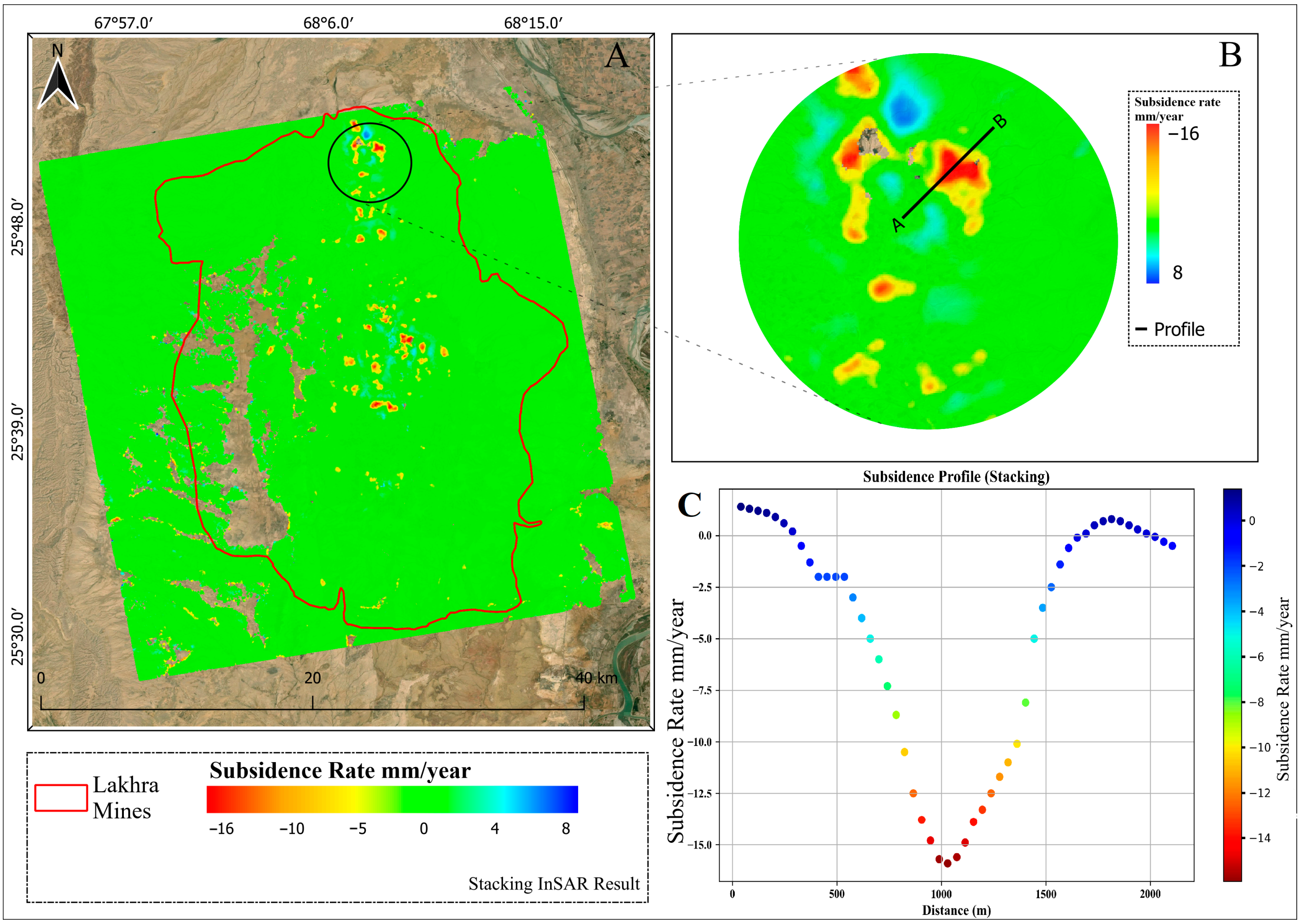

Figure 5. (**A**) Stacking-InSAR Results. (**B**,**C**) Magnified View and Profile Plot, Respectively.

Figure 6A,B shows a magnified view of the highly deformed areas in the UL and LL overlaid on an optical remote sensing image, the areas with maximum and minimum values observed, and the deformation contours, with an interval of 4 mm/year. In total, 33 locations exhibiting deformation in the Upper Lakhra have been identified. Among them, 19 locations show subsidence levels of less than −8 mm/year, while 13 exhibit subsidence levels of more than −8 mm/year. Notably, one location records the highest subsidence value in the Upper Lakhra, reaching −16 mm/year. Additionally, one location exhibits an uplift of 6.8 mm annually (Figure 6A).

Lower Lakhra has been identified to have over 40 locations with deformation, surpassing the deformation level observed in the Upper Lakhra. Among these locations, 15 have subsided at a rate greater than −10 mm/year. The highest recorded subsidence value is −19.4 mm/year, which is the maximum subsidence observed within the entire study area. Additionally, three locations have exhibited an uplift value of around 2–4 mm/year, while the remaining locations have shown a subsidence rate of less than −10 mm/year. Figure 7 shows the enlarged optical satellite imagery of the highly deformed areas of the UL and LL obtained through Google Earth. Different kinds of deformation morphologies can be observed in the image. The blue flag shows the optical view of the area with the maximum value, and the red flags show the optical area view with the minimum value observed in the UL and LL (Figure 7). The polygons show the deformation morphologies of the few deformed areas having substantial deformation values. Every black spot in Figure 7 is either an active or abandoned coal mine or a coal dump.

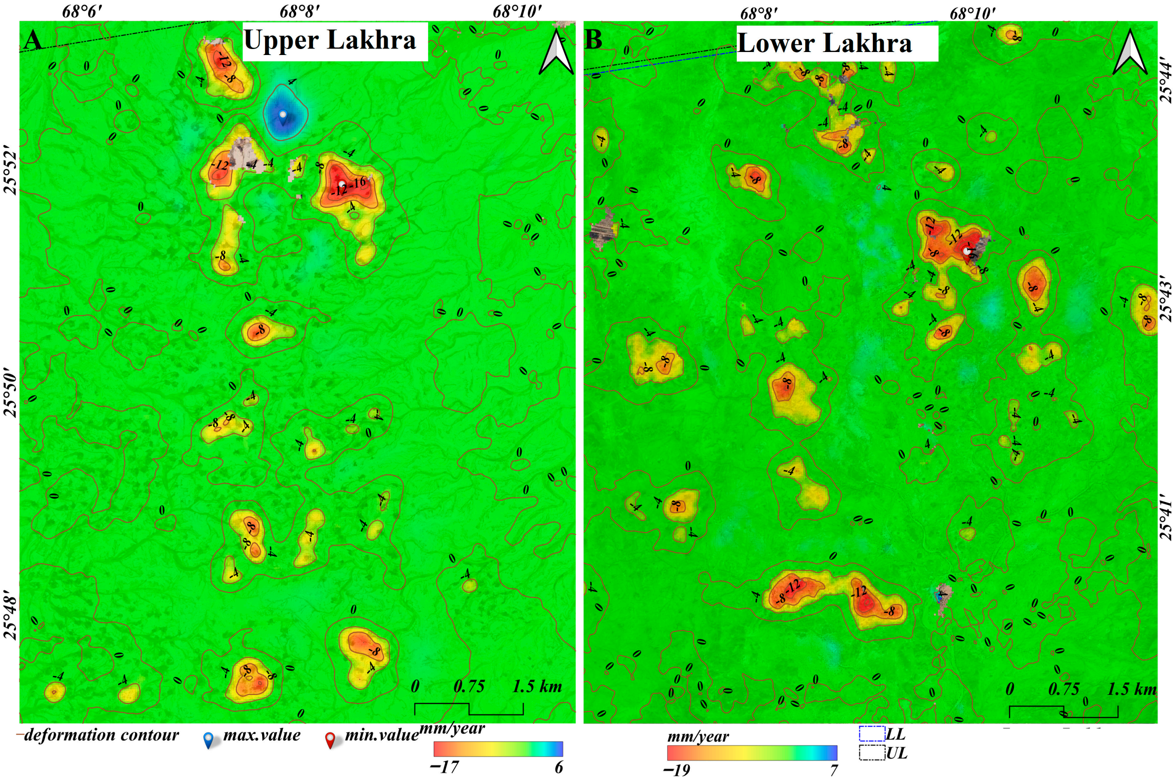

Figure 6. (**A**,**B**) Magnified view of (Stacking) deformation in Upper and Lower Lakhra overlaid on satellite imagery, respectively.

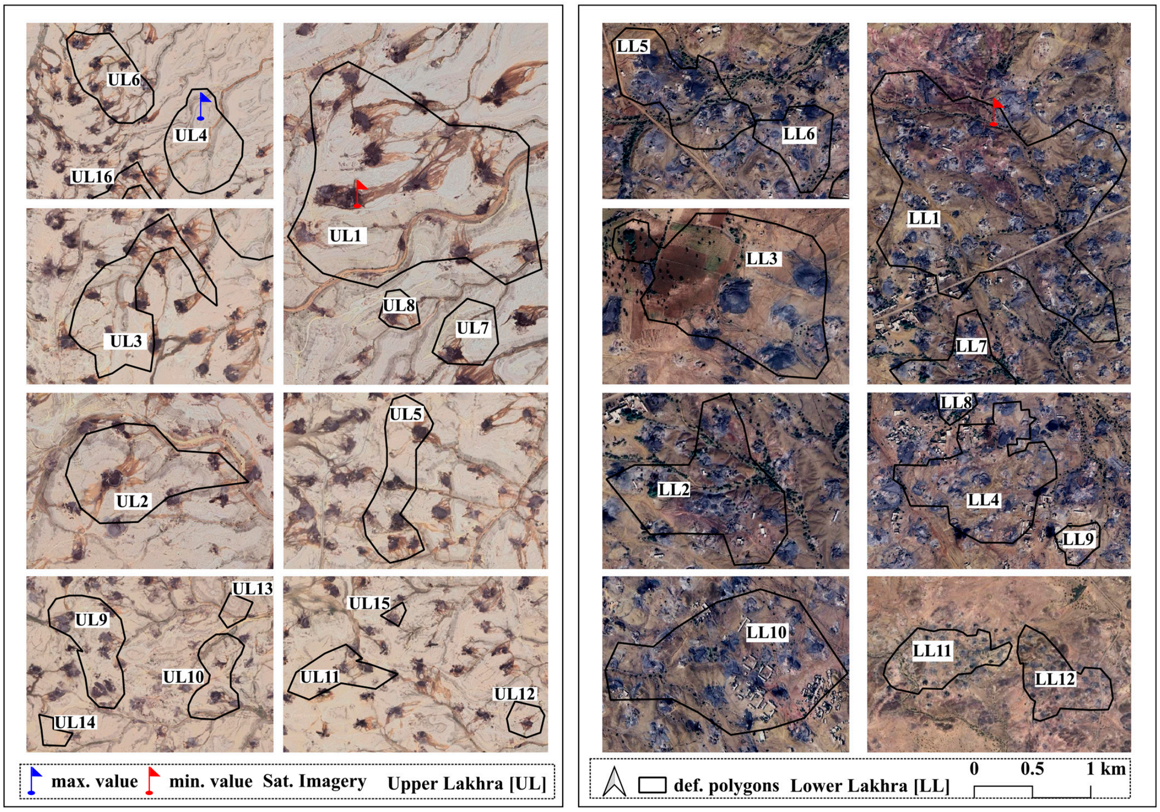

Figure 7. Enlarged Google Earth Image of the Upper (**left side**) and Lower Lakhra (**right side**).

3.2. SBAS-InSAR and Time Series

Figure 8 shows the accumulated deformation in the Lakhra coal area from January 2018 to September 2023. Around 47 locations in the Upper Lakhra exhibit deformation; the accumulated subsidence in the Upper Lakhra is −101 mm. The location showing the highest accumulated subsidence of −101 mm in the UL is marked by a white flag in Figure 8A,B, whereas Figure 8C shows the profile plot along the line (ab). Most of the areas in the UL show accumulative subsidence levels greater than −50 mm. Few spots show uplift in the UL, with the maximum accumulated uplift value reaching up to 28 mm, as marked by a yellow flag in Figures 8A and 9A. The LL location shows 55 deformation spots. The highest accumulated subsidence value observed is −114 mm, as marked by a white flag in Figure 8A and shown in a magnified view in Figure 9B. The maximum accumulated value observed in the LL is 37.39 mm. According to Stacking and SBAS, the LL exhibits more significant deformation and demonstrates the maximum subsidence value within the study area. SBAS-InSAR is limited to monitoring subsidence only at places with a high level of coherence. Due to the high coherence and lack of dense vegetation in our study location, the subsidence areas observed using SBAS-InSAR are greater than those observed using stacking-InSAR. The location of the deformation area, where the most significant subsidence is recorded in both study zones, aligns with the findings from the stacking-InSAR analysis, as observed through SBAS-InSAR. Figure 9A,B shows a magnified view of the Upper and Lower Lakhra area results obtained by SBAS-InSAR and the deformation contours with an interval of 10 mm. Only a few locations showing deformation in the UL and LL are shown in Figure 9A,B. The purpose of SBAS-InSAR is also to obtain the time series deformation in the study area from January 2018 to September 2023; this offers a distinct benefit compared to stacking-InSAR.

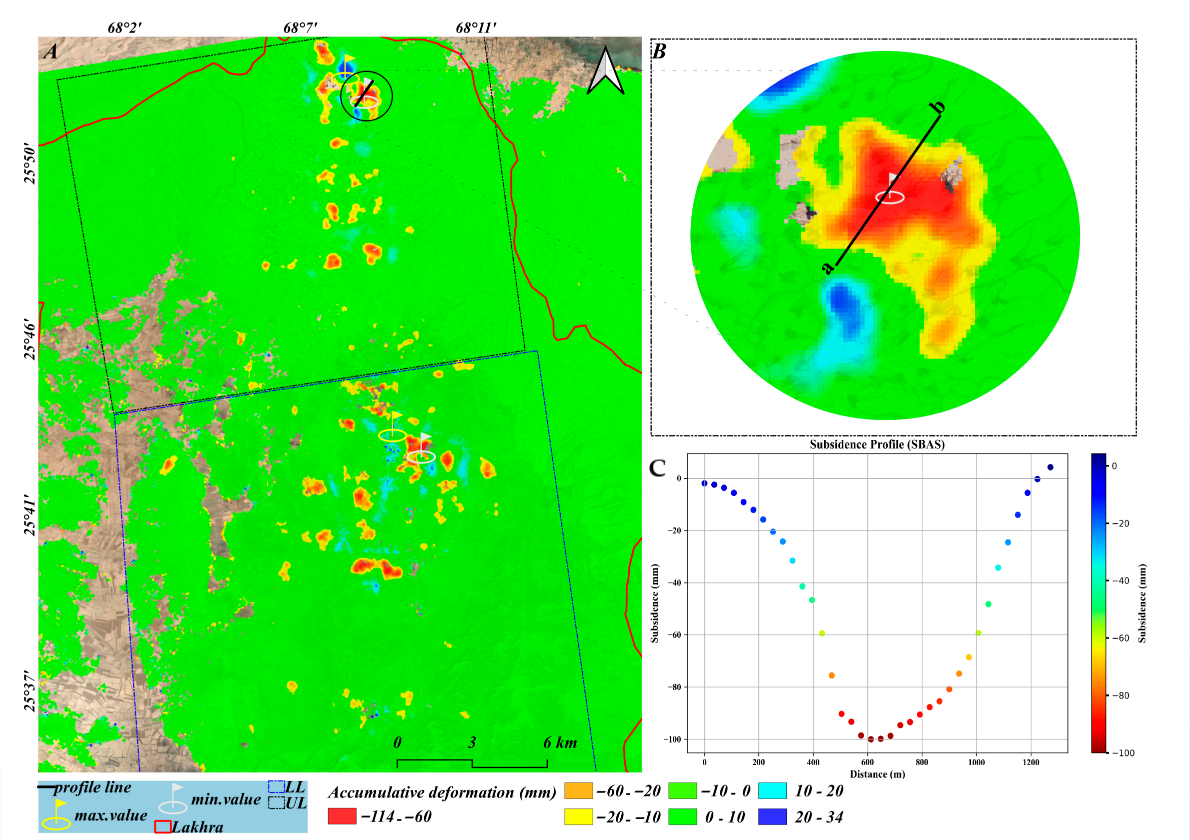

Figure 8. SBAS-InSAR Results. (**A**) Displacement Rates in Lakhra Coal Mines. (**B**,**C**) Magnified View and Profile Plot, Respectively.

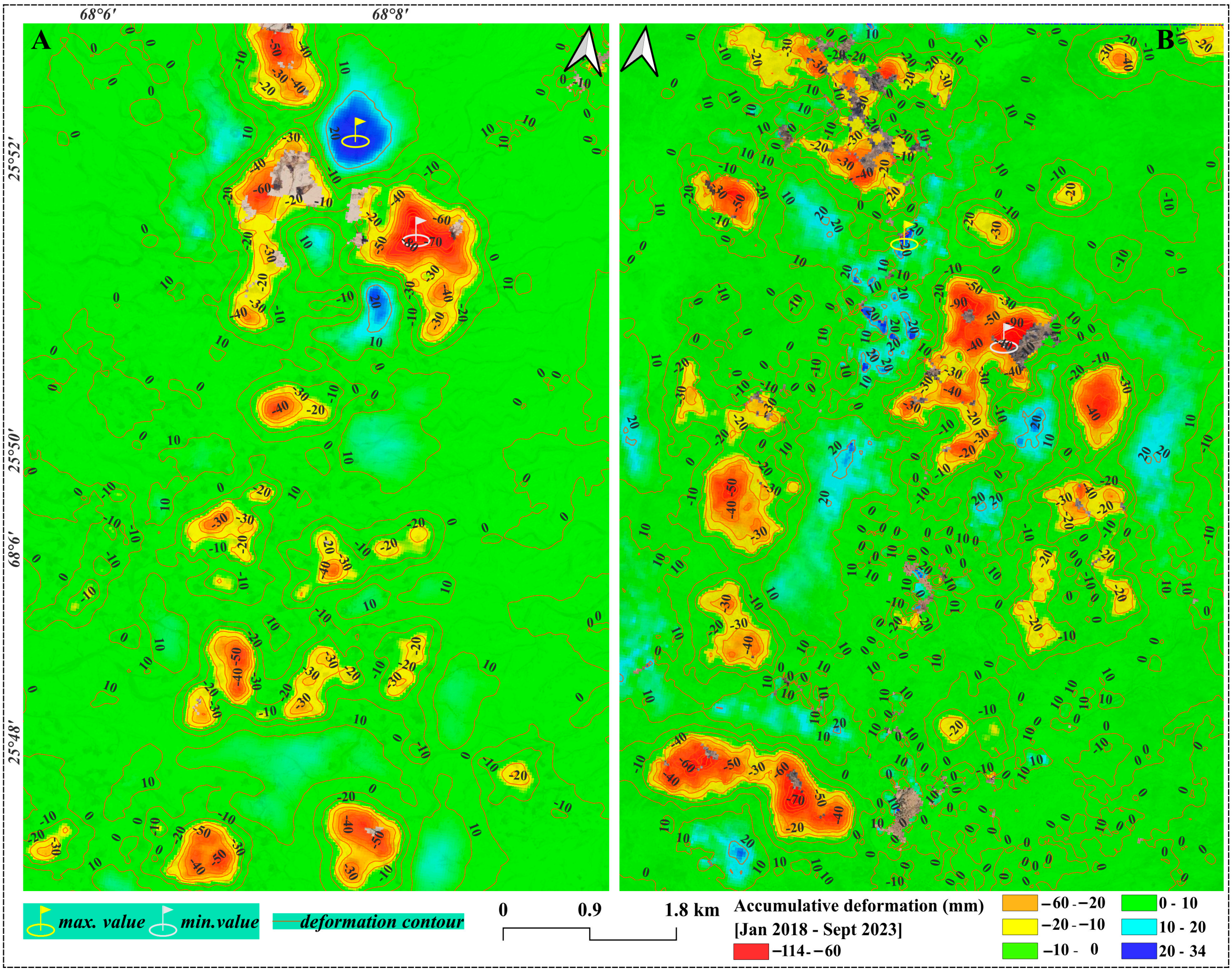

Figure 9. (**A**,**B**) Magnified View of SBAS Accumulative Deformation in the Upper and Lower Lakhra Overlaid on Satellite Imagery, Respectively.

Figure 10 shows the time series deformation obtained by SBAS-InSAR. The research area has experienced increases in the size and scope of subsidence over time. The Lower Lakhra contains the most significant cumulative subsidence values for the investigation. The development of deformation space in the LL is the most significant and has the broadest influence. The maximum subsidence values were consistently recorded in the Lower Lakhra throughout the entire time series analysis.

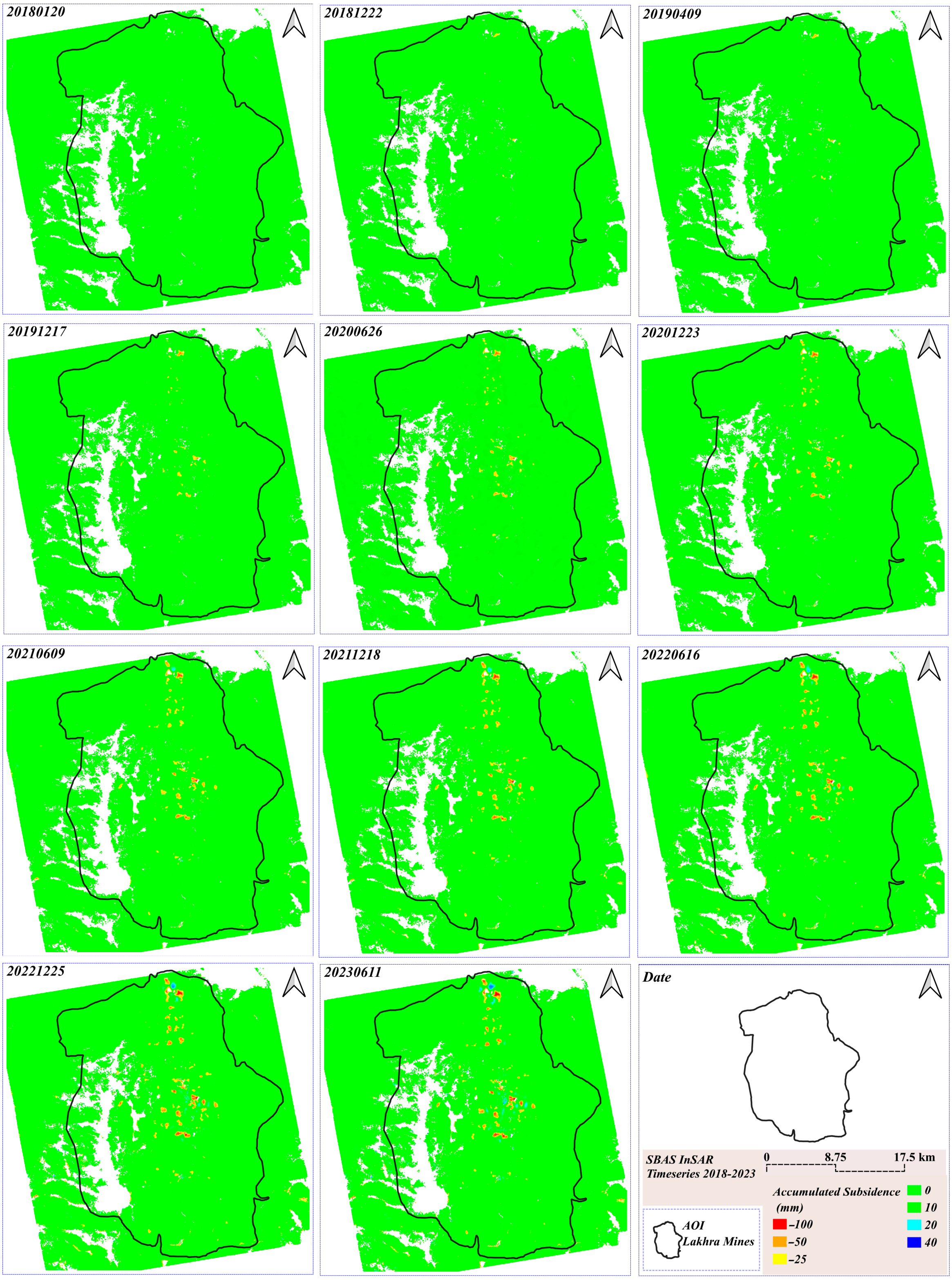

Figure 10. SBAS-InSAR Time Series (2018–2023).

3.3. Zonal Statistics and Quantitative Analysis

We used the land cover raster dataset as a reference to analyze the deformation traits associated with each land cover type and transformed it into vector data. Statistical metrics were computed for each land cover type, encompassing the mean, median, lowest value, highest value, minority representation, majority representation, and standard deviation (SD) shown in Tables 1 and 2.

Table 1. SBAS-InSAR cumulative deformation (mm) statistics for various land cover types.

Land Type	Mean	Median	Stdev	Minimum	Maximum	Minority	Majority
Bare ground	1.11	1.19	5.53	−80.46	28.93	−80.46	−1.37
Rangeland	−0.06	0.48	6.99	−114.02	37.39	−114.02	−43.02
Crop	−5.83	−2.67	11.68	−55.68	17.53	−43.65	−39.54

Table 2. Stacking-InSAR deformation (mm/year) statistics for various land cover types.

Land Type	Mean	Median	Stdev	Minimum	Maximum	Minority	Majority
Bare ground	0.36	0.40	0.95	−14	5.34	−14	0
Rangeland	0.16	0.25	1.20	−19	6.8	−19	−5.10
Crop	−1.04	−0.40	2.05	−7.28	2.71	−6.44	−7.28

The area under consideration amounted to 888.026 square kilometers. Rangeland encompassed the most significant area, comprising 789.05 km^2 or 88.8% of the total; bare ground covered 91.44 km^2 or 10.29%; crops covered 1.10 km^2 or 0.12%; water comprised 0.001 km^2 or 0.000113%; and constructed area accounted for 6.42 km^2 or 0.72%. The efficacy of SBAS-InSAR in less urbanized regions, such as rangelands or rural settings, is typically advantageous owing to its capacity to accurately monitor surface movement in areas with less coherent scatterers [46]. The examination of land deformation obtained from SBAS-InSAR data across different land cover types demonstrates clear and diverse patterns, including more than 400 inactive and operating mines.

The wide-ranging dispersion of data regarding sections of bare ground (Tables 1 and 2), which includes notable rates of both downward (subsidence) and upward (uplift) movement, indicates the presence of several geophysical conditions that are likely impacted by past and current mining operations. Both SBAS- and stacking-InSAR have the highest deformation values in the rangeland. The wide variations in rangeland areas reveal localized subsidence problems that can be ascribed to differential soil compaction, changing vegetation cover, and the impact of mining operations. The considerable fluctuation and substantial downward movement in built areas suggest notable ground displacement, possibly resulting from a mix of human activity, the weight of construction, and destabilization induced by underground mine shafts and tunnels. These data demonstrate the intricate relationships between land cover forms and subsidence rates in an extensively mined region. Each category demonstrates distinct patterns of variation and scale in sinking and rising, emphasizing the significance of considering both surface and subsurface circumstances when evaluating and handling risks and consequences associated with land subsidence.

3.4. Connection between Topographical Elements and Deformation

To comprehend the connection between topographic features and deformation, the Digital Elevation Model was employed to determine aspect, slope, and elevation. The raster-to-point tool created 1,030,244 monitoring points (MPs). Specifically, we examined the subsidence's relationship with slope, elevation, aspect, and the distribution of influential MPs. The results are shown in Figure 11A–C. By using linear regression on subsidence and aspect data, it is found that there is no significant relationship between aspect and subsidence values given the slope value of 0.00. Given an R^2 value of 0.00, it is evident that the linear regression model cannot adequately account for the variations in subsidence values based on the aspect. Based on the low R^2 value, it may be concluded that the linear regression model fails to capture the significant variations in the data shown in Figure 11A. The linear regression analysis of the relationship between subsidence and slope yields a slope of −0.00 and an intercept of −0.07. The R^2 value of 0.00 suggests that the linear regression model is unsuccessful in explaining the variation in subsidence that is dependent on slope. Consequently, a substantial correlation between subsidence and slope values is absent. The proximity of the slope value to zero indicates that variations in slope do not consistently influence the observed subsidence patterns Figure 11B. The linear regression study of subsidence and elevation results in a slope of 0.00 and an intercept of −0.08. The R^2 value of 0.00 suggests that the linear regression model cannot correctly account for the variation in subsidence that depends on elevation. This finding implies that there is an absence of a substantial correlation between subsidence and elevation data. A slope value of 0.00 suggests that elevation variations do not consistently affect the observed subsidence patterns (Figure 11C). Maximum subsidence values are observed at slopes between 0 and 24° and elevations between 30 and 180 m.

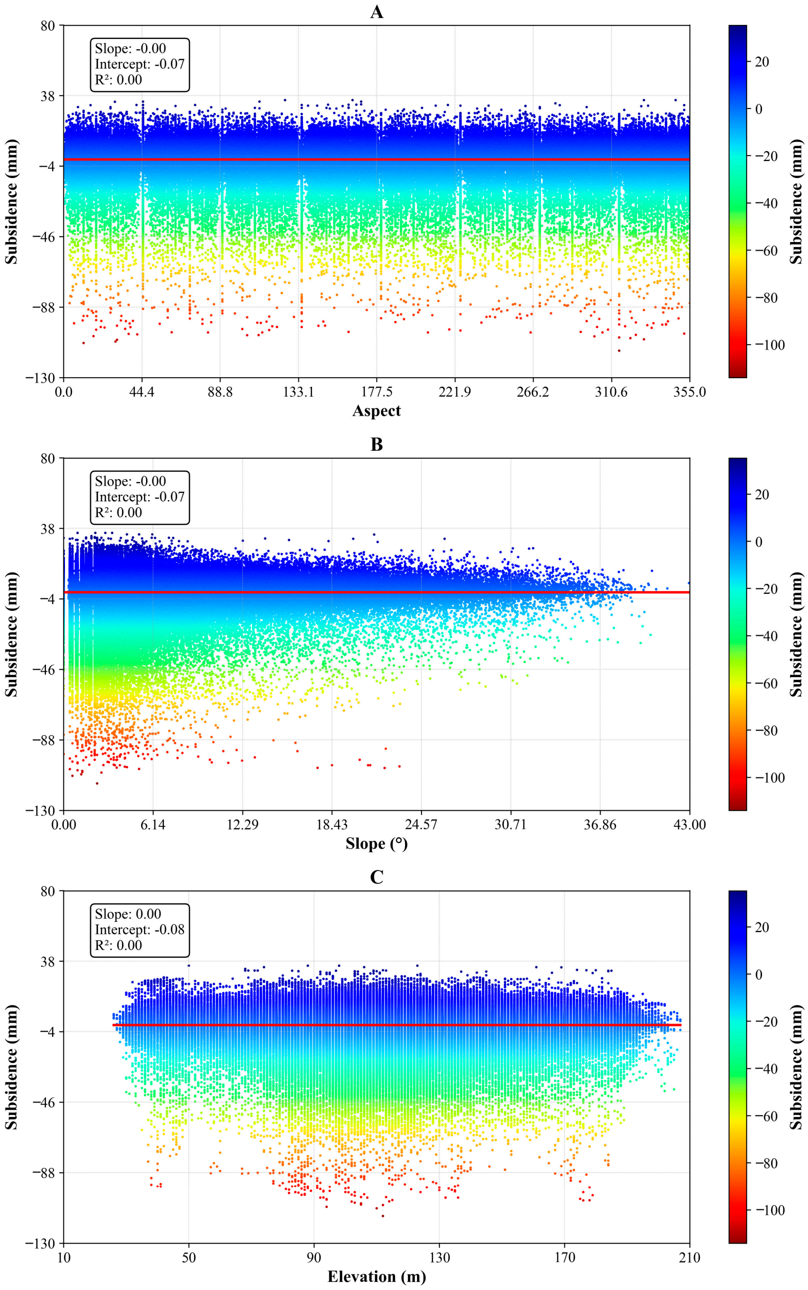

Figure 11. Terrain Factors and SBAS-InSAR Deformation Distribution. (**A**–**C**) Connection of aspect, slope, and elevation with land deformation, respectively.

4. Discussion

4.1. SBAS- and Stacking-InSAR

This study aims to monitor land subsidence in the Lakhra coal mines through cutting-edge SBAS-InSAR and stacking methods. Prior studies have not utilized advanced InSAR methods to detect significant land subsidence in this area, despite the importance of these data in understanding ground deformation in the region. When employing the SBAS-InSAR model, the coherence point selection algorithm is essential in selecting high-coherence points that can sustain high coherence over a specific time [47]. Figure 7 clearly illustrates that the region surrounding the mines predominantly lacks vegetation, making it highly conducive for SBAS-InSAR observations. The SBAS method chooses interferograms with strong coherence to guarantee accurate phase measurements. However, InSAR measurements have inherent limitations, such as decorrelation, making certain areas lack deformation data. Field surveys are a practical approach for addressing missing values in a particular location. Another approach is to combine the results of multiple SAR image sources to perform InSAR measurements [48,49]. The collected deformation data are highly significant, even with a few decoherent zones within the study area. The measurement outcomes offer foundational guidance and insights into subsequent monitoring efforts. Moreover, adopting a sequential adjustment approach enhances these efforts by ensuring more precise and adaptable data interpretation [50]. The SBAS-InSAR in Lakhra coal mines identifies 102 deformation locations, whereas the stacking process identifies 73 locations. For more accurate measurements of linear deformation, stacking-InSAR averages many interferograms to cut down on orbital and atmospheric inaccuracies [41]. The highest subsidence values observed by SBAS- and stacking-InSAR are −114 mm and −19 mm/year, respectively. The processing algorithms used by SBAS- and stacking-InSAR are different, and they both assume distinct assumptions about the deformation behavior. SBAS-InSAR assumes that deformation linearly occurs throughout each time interval between successive SAR observations. On the contrary, stacking-InSAR may utilize various temporal filtering methods that can cause the deformation signal to be smoothed, potentially leading to lower estimates of deformation than SBAS-InSAR [24]. The resolution of the InSAR data, both spatially and temporally, can impact the obtained results. SBAS-InSAR generally works on minor spatial scales and may catch localized deformation patterns more successfully than stacking-InSAR [51].

The precision and applicability of stacking-InSAR and SBAS-InSAR approaches can be better understood by examining the standard deviation of the displacement rate monitored. While the mean stacking-InSAR displacement rate for the current investigation is −0.05 mm/year with a standard deviation of 1.17 mm/year, the mean SBAS displacement rate is −0.07 mm with a standard deviation of 6.63 mm. The results suggest that the SBAS-InSAR method, while effectively capturing the overall deformation over the entire research period, has a higher standard deviation than stacking-InSAR. While the stacking-InSAR lower standard deviation indicates its superior precision under the assumption of linear deformation, the higher standard deviation of SBAS-InSAR may be related to its sensitivity to noise and nonlinear deformation. The standard deviation plots of SBAS- and stacking-InSAR are shown in Figure 12. The time-series trends of the SBAS-InSAR of 10 locations from the Upper and Lower Lakhra regions are shown in Figure 13A,B. The deformation values at the observed locations in the UL and LL show a rising trend over time.

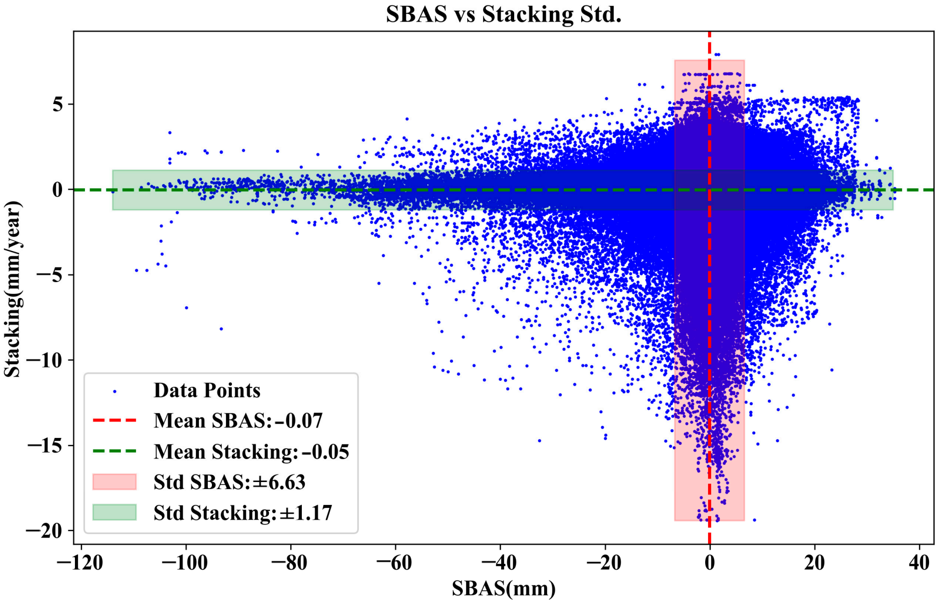

Figure 12. SBAS- and Stacking-InSAR Standard Deviation Plot.

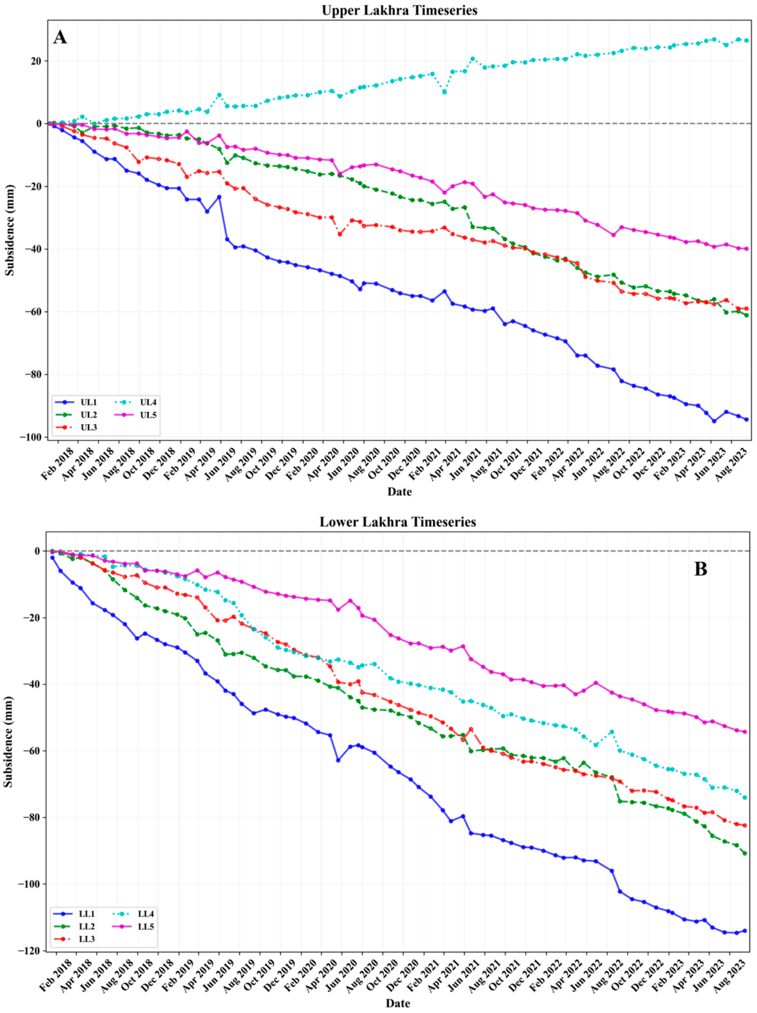

Figure 13. SBAS-InSAR Time-Series Plot of 10 Locations from Upper (**A**) and Lower (**B**) Lakhra Mines.

4.2. Subsidence and Topographic Elements

The correlation between topography and ground deformation in mining regions can be challenging, as mining-induced subsidence is predominantly influenced by subsurface excavation instead of surface topographical traits. This factor distinguishes it from geological dangers such as landslides, which are significantly affected by surface slope and topographical characteristics. The current topographical data analysis indicates that subsidence values are uniformly distributed throughout all aspects, from 0° to 360°, demonstrating an absence of any specific directional pattern associated with the aspect. This characteristic differs from landslide-prone areas, where deformation occurs in particular directions determined by the terrain's aspect and slope. Since there is not any evidence of this trend in the mining area, it is more likely that surface slope and aspect have less influence on subsidence than the depth and placement of underground mining operations. Notably, the most significant subsidence values are seen on very gentle slopes, ranging from 0° to 24°, despite slopes reaching up to 43° in the vicinity. This finding substantiates that subsidence is primarily independent of steep terrain and is more directly associated with underground mining operations' spatial distribution and techniques. Although landslides tend to occur more frequently on steeper slopes, mining-induced subsidence is more likely to occur on gentler slopes, suggesting the presence of underground collapse zones. The widespread occurrence of subsidence at different elevations underscores that elevation is not a critical determinant in this context, reinforcing the idea that subterranean mining activities are the principal cause of surface deformation. Additionally, although topographical parameters like elevation and slope are not directly correlated with mining-induced subsidence, it is essential to understand that over time, subsidence can have a substantial impact on surface topography. This continuous deformation may intensify surface characteristics, such as slight inclines and drainage patterns, possibly resulting in further environmental repercussions.

4.3. Subsidence and Mining Activities

The region in Lower Lakhra exhibiting significant subsidence values is examined through Google Earth imagery from 2018 to 2023 to elucidate the relationship between mining operations and subsidence. In 2018, there were few mining sites; nevertheless, by 2023, the number of operational mines and their spatial extent had significantly expanded, as illustrated in Figure 14A,B. In contrast, Figure 14C,D shows the increase in subsidence values in the same area from 2018 to 2023. The rapid subsidence in the Lower Lakhra is likely accelerated by the expansion of mining regions and extends in several ways. (1) Expanded extraction zones generate more substantial subterranean cavities, heightening the likelihood of ground subsidence and surface distortion. (2) Expanding mines frequently connect with previously excavated regions, exacerbating destabilization and resulting in accelerated sinking. (3) Expanded mining footprints disrupt a larger surface area, increasing land exposure to prospective subsidence risks. The choice of mining processes, such as pillar mining, longwall mining, or room and pillar mining, can impact the degree of subsidence in mining regions. The selection of mining methodology affects the terrain's stability and the likelihood of subsidence [52,53]. Surface mining operations and the removal and disposal of overlying soil and rock result in land cover alterations and land utilization in mining regions, leading to subsidence [54]. Coal field closures and flooding can result in the upward movement of the surface [55,56]. Significant uplift in mining regions may transpire because of stress redistribution after mineral extraction, resulting in initial subsidence succeeded by rebound upon the cessation of mining activities. Abandoned areas (goafs) may initially subside and subsequently rise as adjacent materials realign. Moreover, environmental modifications, such as land reclamation and forest restoration, can disrupt hydrological balances and facilitate elevation [57]. Moreover, dependence on antiquated mining methods in the Lower Lakhra intensifies subsidence problems. Shaft mining Figure 15 and manual coal drilling exhibit lower efficiency and frequently lack contemporary safety protocols that can alleviate subsidence hazards. These approaches often disrupt extensive geographical areas without sufficient support structures, heightening the risk of ground instability. Furthermore, the human coal drilling technique is inferior in precision and efficiency to mechanized techniques, resulting in possible over-extraction and increased ground destabilization.

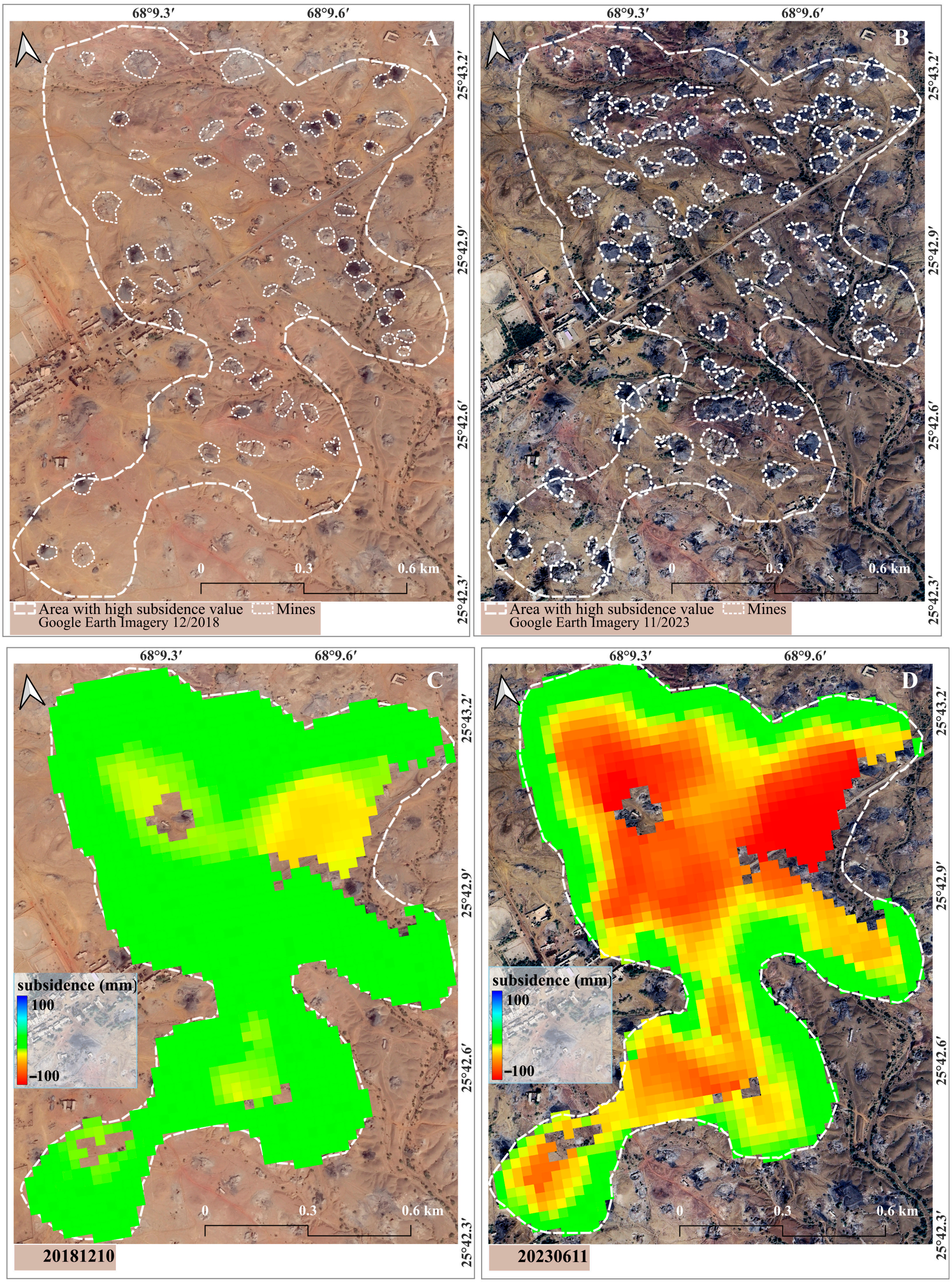

Figure 14. Expansion of Mines and Subsidence in the Lower Lakhra in 2018–2023. (**A**,**B**) Google Earth images of mines from 2018–2023 (**C**,**D**) subsidence observed during 2018–2023.

Figure 15. Shaft Mining in Lakhra Coal Mines. Source: Mineral Transformation Plan Vision 2025, Government of Pakistan.

The aggregate impacts of intensified mining operations, along with antiquated methods, have resulted in concerning levels of subsidence. The amalgamation of enlarged mining zones and heightened extraction activities establishes a feedback cycle wherein each new activity amplifies susceptibility to ground displacement. Research indicates that areas with a history of intensive mining frequently undergo considerable subsidence long after the cessation of activities, which is attributable to the delayed collapse of subterranean supports [58].

It is hypothesized that the deformation in the study area results from extensive mining based on the area's optical picture and local geographical characteristics. These results align with the expected effects of underground mining activities, which generate surface deformation by extracting underlying material. The subsidence is primarily in areas directly atop and near the mining operations. Coal production has been increasing in Pakistan in recent years, as seen in Figure 16. Mining operations, specifically underground coal mining, may have resulted in ground instability and surface deformation due to extracting resources from the earth.

Numerous articles have addressed whether the deformation in the LOS direction accurately represents the movement of the ground surface [44,59,60]. The observed subsidence has essential ramifications for mining area environmental control and infrastructure. Thus, early risk identification and mitigation rely on continuous InSAR monitoring, the need for more environmentally friendly mining methods, and adequate ground support regulations. Even though the InSAR methods used worked well in our study, some limitations must be acknowledged. First, atmospheric artifacts, orbital errors, unwrapping errors, spatial and temporal resolution errors, and signal decorrelation can change how accurate InSAR results are, especially in places with a lot of vegetation or water. Even after applying conventional corrections, residual errors may still exist. The second issue is that quick subsidence events between observation intervals are difficult to catch due to the limited temporal resolution of satellite acquisitions. This research primarily concentrates on line-of-sight deformation assessments. Owing to the restricted accessibility of data sources, namely the lack of Global Navigation Satellite System (GNSS) measurements or relevant information on subsidence in the area of interest, we lack corroborative evidence for zero horizontal motion across the entire research area or its specific segments.

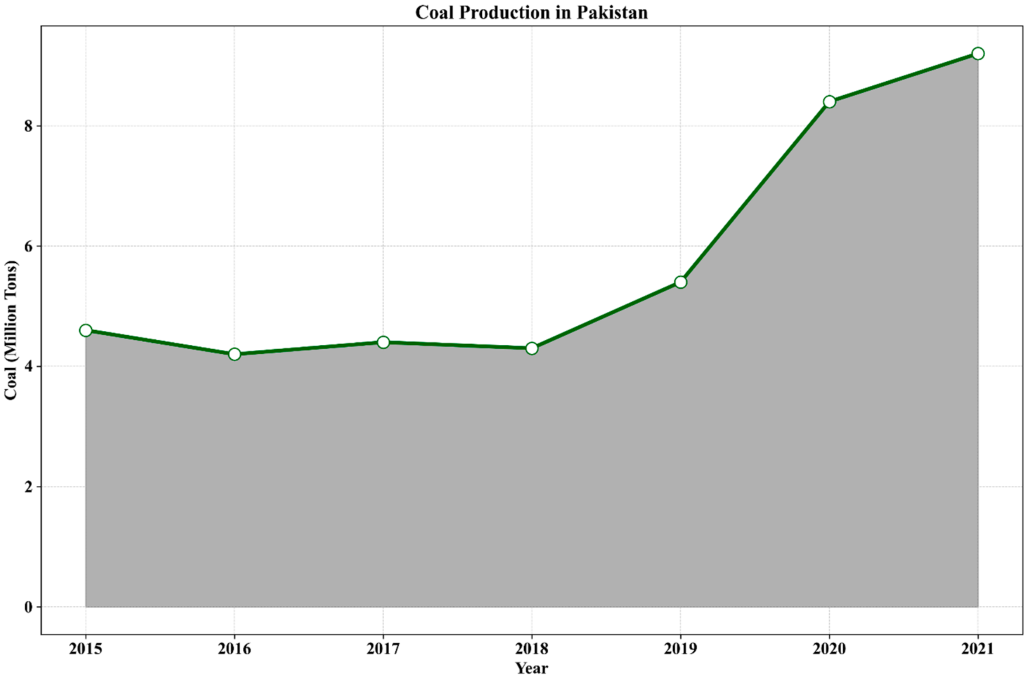

Figure 16. Coal Production in Pakistan. Source: BP Statistical Review 2022 and Pakistan Energy Yearbook 2022.

Integrating information with higher temporal resolution or supplementary ground-based monitoring methods like GPS can enhance future investigations. Monitoring subsidence should be improved by enhancing its temporal and spatial resolution in the future. In addition to InSAR, other geodetic techniques, such as terrestrial laser scanning (TLS) or unmanned aerial vehicle photogrammetry, may offer more detailed information about deformation mechanisms. Advanced atmospheric correction algorithms and machine learning techniques can further enhance InSAR measurements. Long-term monitoring is critical for understanding subsidence and evaluating the effectiveness of mitigation strategies.

5. Conclusions

This study is the first to employ the SBAS-InSAR and stacking-InSAR methods using 150 ascending Sentinel-1A data to investigate surface deformation in the Lakhra coal mine in Sindh Province, Pakistan, as no prior studies or subsidence identification methods have been employed. Although the SBAS-InSAR technique is well-established, its utilization in this unexplored area underscores its efficacy in identifying mining-induced ground displacement. The cumulative count of regions exhibiting deformation using InSAR stacking is 73, while SBAS-InSAR identifies 102 deformation locations. The greatest magnitude is observed at the Lower Lakhra, where the subsidence is measured at approximately −114 mm by SBAS-InSAR and at a rate of around −19 mm/year through stacking-InSAR. The Lower Lakhra exhibits greater deformation than the Upper Lakhra, characterized by higher deformation values and a more considerable extent of affected zones. Our investigation indicates that deformation trends are primarily unaffected by topographic parameters such as slope aspect and elevation. Most of the region under investigation is composed of rangeland, which accounts for 88.8% of the entire area and exhibits the highest levels of deformation. The SBAS-InSAR method identifies a greater subsidence rate in the line-of-sight direction than the stacking-InSAR method due to the highly coherent spots in the study area. The optical remote sensing images are used to quantify the cause of subsidence. All the deformation locations identified are around or over mines. Coal production in Pakistan has increased, and intense mining has caused land subsidence. Intensive coal resource mining can destabilize the soil's geological composition, resulting in empty spaces and hollow areas underground. These empty spaces are prone to collapse without sufficient support or reinforcement, resulting in subsidence. Moreover, using inadequate mining techniques intensifies the land subsidence hazards linked to coal mining. Practices such as insufficient backfilling, incorrect excavation practices, and the absence of structural reinforcing can expedite the destabilization of the land. The confluence of rigorous coal extraction with substandard mining techniques presents substantial environmental and socioeconomic hazards, jeopardizing not only the stability of the terrain but also adjacent infrastructure, ecosystems, and communities. To minimize the detrimental effects of land subsidence caused by coal mining, it is crucial to implement responsible mining methods, sustainable practices, and strict regulatory supervision. This is necessary to protect the environment and human settlements from the harmful repercussions of subsidence. The results establish a fundamental comprehension of subsidence in that area and underscore the necessity of ongoing monitoring and additional research. These initial findings can be further developed using this technique to investigate additional mining regions or obtain higher-resolution data in future studies. Future research should prioritize integrating additional on-site monitoring data to strengthen validation and improve the precision of subsidence measures.

Author Contributions: Conceptualization, T.A. and F.Y.; methodology, T.A. and F.Y.; software, T.A.; validation, L.L. and F.Y.; writing—original draft, T.A.; writing—review and editing, L.L., F.Y. and Q.Z.; visualization, T.A.; supervision, L.L. All authors have read and agreed to the published version of the manuscript.

Funding: We extend our gratitude to the National Natural Science Foundation of China (42071258) and the Natural Science Basic Research Program of Shaanxi Province (Grant No. 2023-JC-ZD-18, 2024SF-YBXM-570) for their support in funding this study.

Data Availability Statement: The data presented in the study are available on request from the first author. The data are not publicly available due to the thesis that is being prepared from these data.

Acknowledgments: We thank the Alaska Satellite Facility (ASF) for free Sentinel-1 data and USGS Earth Explorer for providing DEM data. We sincerely thank the reviewers for their time, effort, and valuable insights. Their constructive feedback has been instrumental in significantly enhancing the quality of our manuscript.

Conflicts of Interest: The authors declare no conflicts of interest.

References

1. Raspini, F.; Bianchini, S.; Moretti, S.; Loupasakis, C.; Rozos, D.; Duro, J.; Garcia, M. Advanced interpretation of interferometric SAR data to detect, monitor and model ground subsidence: Outcomes from the ESA-GMES Terrafirma project. *Nat. Hazards* **2016**, *83*, 155–181. [CrossRef]
2. Zhang, Y.; Liu, Y.; Jin, M.; Jing, Y.; Liu, Y.; Liu, Y.; Sun, W.; Wei, J.; Chen, Y. Monitoring land subsidence in Wuhan city (China) using the SBAS-InSAR method with radarsat-2 imagery data. *Sensors* **2019**, *19*, 743. [CrossRef] [PubMed]
3. Li, D.; Li, B.; Zhang, Y.; Fan, C.; Xu, H.; Hou, X. Spatial and temporal characteristics analysis for land subsidence in Shanghai coastal reclamation area using PS-InSAR method. *Front. Mar. Sci.* **2022**, *9*, 1000523. [CrossRef]
4. Zhang, Z.; Hu, C.; Wu, Z.; Zhang, Z.; Yang, S.; Yang, W. Monitoring and analysis of ground subsidence in Shanghai based on PS-InSAR and SBAS-InSAR technologies. *Sci. Rep.* **2023**, *13*, 8031. [CrossRef]
5. Wang, F.; Tao, Q.; Liu, G.; Chen, Y.; Han, Y.; Guo, Z.; Liu, X. Monitoring of surface deformation in mining area integrating SBAS InSAR and Logistic Function. *Environ. Monit. Assess.* **2023**, *195*, 1493. [CrossRef] [PubMed]
6. Liu, X.; Xing, X.; Wen, D.; Chen, L.; Yuan, Z.; Liu, B.; Tan, J. Mining-induced time-series deformation investigation based on SBAS-InSAR technique: A case study of drilling water solution rock salt mine. *Sensors* **2019**, *19*, 5511. [CrossRef]

7. Fielding, E.J.; Blom, R.G.; Goldstein, R.M. Rapid subsidence over oil fields measured by SAR interferometry. *Geophys. Res. Lett.* **1998**, *25*, 3215–3218. [CrossRef]
8. Gabriel, A.K.; Goldstein, R.M.; Zebker, H.A. Mapping small elevation changes over large areas: Differential radar interferometry. *J. Geophys. Res. Solid Earth* **1989**, *94*, 9183–9191. [CrossRef]
9. Zebker, H.A.; Villasenor, J. Decorrelation in interferometric radar echoes. *IEEE Trans. Geosci. Remote Sens.* **1992**, *30*, 950–959. [CrossRef]
10. Hanssen, R.F. *Radar Interferometry: Data Interpretation and Error Analysis*; Springer Science & Business Media: Dordrecht, The Netherlands, 2001; Volume 2.
11. Ferretti, A.; Prati, C.; Rocca, F. Nonlinear subsidence rate estimation using permanent scatterers in differential SAR interferometry. *IEEE Trans. Geosci. Remote Sens.* **2000**, *38*, 2202–2212. [CrossRef]
12. Ferretti, A.; Prati, C.; Rocca, F. Permanent scatterers in SAR interferometry. *IEEE Trans. Geosci. Remote Sens.* **2001**, *39*, 8–20. [CrossRef]
13. Usai, S. A New Approach for Longterm Monitoring of Deformations by Differential SAR Interferometry. Ph.D. Thesis, Delft University of Technology, Delft, The Netherlands, 2001.
14. Chen, X.; Tessari, G.; Fabris, M.; Achilli, V.; Floris, M. Comparison between PS and SBAS InSAR techniques in monitoring shallow landslides. In *Understanding and Reducing Landslide Disaster Risk: Volume 3 Monitoring and Early Warning*, 5th ed.; Springer: Cham, Switzerland, 2021; pp. 155–161.
15. Zhang, P.; Qian, X.; Guo, S.; Wang, B.; Xia, J.; Zheng, X. A New Method for Continuous Track Monitoring in Regions of Differential Land Subsidence Rate Using the Integration of PS-InSAR and SBAS-InSAR. *Remote Sens.* **2023**, *15*, 3298. [CrossRef]
16. Casu, F.; Manzo, M.; Lanari, R. A quantitative assessment of the SBAS algorithm performance for surface deformation retrieval from DInSAR data. *Remote Sens. Environ.* **2006**, *102*, 195–210. [CrossRef]
17. Hu, B.; Wang, H.-S.; Sun, Y.-L.; Hou, J.-G.; Liang, J. Long-term land subsidence monitoring of Beijing (China) using the small baseline subset (SBAS) technique. *Remote Sens.* **2014**, *6*, 3648–3661. [CrossRef]
18. Loesch, E.; Sagan, V. SBAS analysis of induced ground surface deformation from wastewater injection in East Central Oklahoma, USA. *Remote Sens.* **2018**, *10*, 283. [CrossRef]
19. Wu, Q.; Jia, C.; Chen, S.; Li, H. SBAS-InSAR based deformation detection of urban land, created from mega-scale mountain excavating and valley filling in the Loess Plateau: The case study of Yan'an City. *Remote Sens.* **2019**, *11*, 1673. [CrossRef]
20. Zhao, F.; Meng, X.; Zhang, Y.; Chen, G.; Su, X.; Yue, D. Landslide susceptibility mapping of karakorum highway combined with the application of SBAS-InSAR technology. *Sensors* **2019**, *19*, 2685. [CrossRef] [PubMed]
21. Su, X.; Zhang, Y.; Meng, X.; Rehman, M.U.; Khalid, Z.; Yue, D. Updating inventory, deformation, and development characteristics of landslides in Hunza Valley, NW Karakoram, Pakistan by SBAS-InSAR. *Remote Sens.* **2022**, *14*, 4907. [CrossRef]
22. Milczarek, W. Investigation of post inducted seismic deformation of the 2016 Mw4. 2 tarnowek Poland mining tremor based on Dinsar and SBAS methods. *Acta Geodyn. Geomat.* **2019**, *16*, 194.
23. Parwata, I.N.S.; Nakashima, S.; Shimizu, N. Monitoring volcanic activity of Mount Agung, Indonesia by SBAS-DInSAR using Sentinel-1 data from 2014 to 2020. In *Rock Mechanics and Engineering Geology in Volcanic Fields*; CRC Press: Boca Raton, FL, USA, 2022; pp. 50–57.
24. Chen, Y.; Tong, Y.; Tan, K. Coal mining deformation monitoring using SBAS-InSAR and offset tracking: A case study of Yu County, China. *IEEE J. Sel. Top. Appl. Earth Obs. Remote Sens.* **2020**, *13*, 6077–6087. [CrossRef]
25. Du, Q.; Li, G.; Chen, D.; Zhou, Y.; Qi, S.; Wu, G.; Chai, M.; Tang, L.; Jia, H.; Peng, W. SBAS-InSAR-Based analysis of surface deformation in the eastern tianshan mountains, China. *Front. Earth Sci.* **2021**, *9*, 729454. [CrossRef]
26. Dai, K.; Liu, G.; Li, Z.; Ma, D.; Wang, X.; Zhang, B.; Tang, J.; Li, G. Monitoring highway stability in permafrost regions with X-band temporary scatterers stacking InSAR. *Sensors* **2018**, *18*, 1876. [CrossRef] [PubMed]
27. Sandwell, D.T.; Price, E.J. Phase gradient approach to stacking interferograms. *J. Geophys. Res. Solid Earth* **1998**, *103*, 30183–30204. [CrossRef]
28. Strozzi, T.; Wegmuller, U.; Werner, C.; Wiesmann, A. Measurement of slow uniform surface displacement with mm/year accuracy. In Proceedings of the IGARSS 2000—IEEE 2000 International Geoscience and Remote Sensing Symposium—Taking the Pulse of the Planet: The Role of Remote Sensing in Managing the Environment, Proceedings (Cat. No. 00CH37120), Honolulu, HI, USA, 24–28 July 2000; pp. 2239–2241.
29. Zhao, Q.; Lin, H.; Jiang, L. Ground deformation monitoring in Pearl River Delta region with Stacking D-InSAR technique. In Proceedings of the Geoinformatics 2008 and Joint Conference on GIS and Built Environment: Monitoring and Assessment of Natural Resources and Environments, Guangzhou, China, 3 November 2008; pp. 366–374.
30. Qin, Z.; Agarwal, V.; Gee, D.; Marsh, S.; Grebby, S.; Chen, Y.; Meng, N. Study of ground movement in a mining area with geological faults using FDM analysis and a stacking InSAR method. *Front. Environ. Sci.* **2021**, *9*, 787053. [CrossRef]
31. Jiang, L.; Lin, H.; Ma, J.; Kong, B.; Wang, Y. Potential of small-baseline SAR interferometry for monitoring land subsidence related to underground coal fires: Wuda (Northern China) case study. *Remote Sens. Environ.* **2011**, *115*, 257–268. [CrossRef]
32. Zhu, Y.; Yao, X.; Yao, L.; Yao, C. Detection and characterization of active landslides with multisource SAR data and remote sensing in western Guizhou, China. *Nat. Hazards* **2022**, *111*, 973–994. [CrossRef]
33. Maaß, A.-L.; Schüttrumpf, H. Long-term effects of mining-induced subsidence on the trapping efficiency of floodplains. *Anthropocene* **2018**, *24*, 1–13. [CrossRef]

34. Bazaluk, O.; Kuchyn, O.; Saik, P.; Soltabayeva, S.; Brui, H.; Lozynskyi, V.; Cherniaiev, O. Impact of ground surface subsidence caused by underground coal mining on natural gas pipeline. *Sci. Rep.* **2023**, *13*, 19327. [CrossRef] [PubMed]
35. Shahani, N.; Wan, Z.; Ali, M.; Ullah, B. Detection and monitoring of underground coal mine gases at Lakhra Coal Mines, Pakistan. In Proceedings of the 35th Annual International Pittsburgh Conference, Xuzhou, China, 15–18 October 2018; pp. 1–8.
36. Sanjrani, M.; Memon, I.; Awan, B. Environmental Impact of Lakhra Coal Mining, Sindh province, Pakistan. *N. Am. Acad. Res.* **2018**, *1*, 72–75.
37. Guo, J.; Hu, J.; Li, B.; Zhou, L.; Wang, W. Land subsidence in Tianjin for 2015 to 2016 revealed by the analysis of Sentinel-1A with SBAS-InSAR. *J. Appl. Remote Sens.* **2017**, *11*, 026024. [CrossRef]
38. Ferretti, A.; Monti-Guarnieri, A.; Prati, C.; Rocca, F.; Massonet, D. *SAR Principles-Guidelines for SAR Interferometry Processing and Interpretation*; European Space Agency: Paris, France, 2007; Volume 19.
39. Berardino, P.; Fornaro, G.; Lanari, R.; Sansosti, E. A new algorithm for surface deformation monitoring based on small baseline differential SAR interferograms. *IEEE Trans. Geosci. Remote Sens.* **2002**, *40*, 2375–2383. [CrossRef]
40. Schmidt, D.A.; Bürgmann, R. Time-dependent land uplift and subsidence in the Santa Clara valley, California, from a large interferometric synthetic aperture radar data set. *J. Geophys. Res. Solid Earth* **2003**, *108*. [CrossRef]
41. Lanari, R.; Mora, O.; Manunta, M.; Mallorquí, J.J.; Berardino, P.; Sansosti, E. A small-baseline approach for investigating deformations on full-resolution differential SAR interferograms. *IEEE Trans. Geosci. Remote Sens.* **2004**, *42*, 1377–1386. [CrossRef]
42. Hooper, A. A multi-temporal InSAR method incorporating both persistent scatterer and small baseline approaches. *Geophys. Res. Lett.* **2008**, *35*. [CrossRef]
43. Yan, Y.; Doin, M.-P.; Lopez-Quiroz, P.; Tupin, F.; Fruneau, B.; Pinel, V.; Trouvé, E. Mexico City subsidence measured by InSAR time series: Joint analysis using PS and SBAS approaches. *IEEE J. Sel. Top. Appl. Earth Obs. Remote Sens.* **2012**, *5*, 1312–1326. [CrossRef]
44. Hu, J.; Li, Z.; Zhu, J.; Liu, J. *Theory and Application of Monitoring 3-D Deformation with InSAR*; Science Press: Beijing, China, 2021; ISBN 978-7-03-068643-5.
45. Wegnüller, U.; Werner, C.; Strozzi, T.; Wiesmann, A.; Frey, O.; Santoro, M. Sentinel-1 support in the GAMMA software. *Procedia Comput. Sci.* **2016**, *100*, 1305–1312. [CrossRef]
46. Huang, G.; Dong, J.; Xi, W.; Zhao, Z.; Li, S.; Kuang, Z.; An, Q.; Wei, J.; Zhu, Y. Study on surface deformation pattern in mine closure area of complex karst mountainous region based on SBAS-InSAR technology. *Front. Earth Sci.* **2024**, *11*, 1353593. [CrossRef]
47. Xu, Y.; Li, T.; Tang, X.; Zhang, X.; Fan, H.; Wang, Y. Research on the applicability of DInSAR, stacking-InSAR and SBAS-InSAR for mining region subsidence detection in the datong coalfield. *Remote Sens.* **2022**, *14*, 3314. [CrossRef]
48. Guo, N.; Zhan, W. Research on the method of three-dimensional surface displacements of Tianjin area based on combined multi-source measurements. *J. Appl. Geod.* **2020**, *14*, 83–94. [CrossRef]
49. Jianjun, Z.; Zefa, Y.; Zhiwei, L. Recent progress in retrieving and predicting mining-induced 3D displace-ments using InSAR. *Acta Geod. Cartogr. Sin.* **2019**, *48*, 135.
50. Wang, H.; Zeng, Q.; Jiao, J.; Chen, J. InSAR Time Series Analysis Technique Combined with Sequential Adjustment Method for Monitoring of Surface Deformation. *Beijing Da Xue Xue Bao* **2021**, *57*, 241–249.
51. Gong, W.; Thiele, A.; Hinz, S.; Meyer, F.J.; Hooper, A.; Agram, P.S. Comparison of small baseline interferometric SAR processors for estimating ground deformation. *Remote Sens.* **2016**, *8*, 330. [CrossRef]
52. Li, Z.; Tian, Z.; Wang, B.; Li, W.; Chen, Q.; Zhang, Z. Monitoring and Assessment of SBAS-InSAR Deformation for Sustainable Development of Closed Mining Areas—A Case of Nanzhuang Mining Area. *IEEE Access* **2023**, *11*, 22935–22947. [CrossRef]
53. Chen, D.; Chen, H.; Zhang, W.; Cao, C.; Zhu, K.; Yuan, X.; Du, Y. Characteristics of the residual surface deformation of multiple abandoned mined-out areas based on a field investigation and SBAS-InSAR: A case study in Jilin, China. *Remote Sens.* **2020**, *12*, 3752. [CrossRef]
54. Eker, R.; Aydın, A.; Görüm, T. Tracking deformation velocity via PSI and SBAS as a sign of landslide failure: An open-pit mine-induced landslide in Himmetoğlu (Bolu, NW Turkey). *Nat. Hazards* **2024**, *120*, 7701–7724. [CrossRef]
55. Vervoort, A. Uplift of the surface of the earth above abandoned coal mines. Part B: Framework to understand and explain uplift. *Int. J. Rock Mech. Min. Sci.* **2021**, *148*, 104947. [CrossRef]
56. Vervoort, A. Uplift of the surface of the earth above abandoned coal mines. Part A: Analysis of satellite data related to the movement of the surface. *Int. J. Rock Mech. Min. Sci.* **2021**, *148*, 104896. [CrossRef]
57. Zheng, L.; Zhu, L.; Wang, W.; Guo, L.; Chen, B. Land subsidence related to coal mining in China revealed by L-band InSAR analysis. *Int. J. Environ. Res. Public Health* **2020**, *17*, 1170. [CrossRef] [PubMed]
58. Fan, H.; Wang, L.; Wen, B.; Du, S. A new model for three-dimensional deformation extraction with single-track InSAR based on mining subsidence characteristics. *Int. J. Appl. Earth Obs. Geoinf.* **2021**, *94*, 102223. [CrossRef]
59. Chen, F.; Lin, H.; Zhou, W.; Hong, T.; Wang, G. Surface deformation detected by ALOS PALSAR small baseline SAR interferometry over permafrost environment of Beiluhe section, Tibet Plateau, China. *Remote Sens. Environ.* **2013**, *138*, 10–18. [CrossRef]
60. Ge, W.; Li, Y.; Wang, Z.; Zhang, C.; Yang, H. Spatial-Temporal Ground Deformation Study of Baotou Based on the PS-InSAR Method. *Acta Geol. Sin.-Engl. Ed.* **2021**, *95*, 674–683. [CrossRef]